Catalysis Today 377 (2021) 157–165

Contents lists available at ScienceDirect

Catalysis Today

journal homepage: www.elsevier.com/locate/cattod

Copper sulfide derived nanoparticles supported on carbon for the electrochemical reduction of carbon dioxide

Christina H.M. van Oversteeg [a,b,1], Marisol Tapia Rosales [a,1], Kristiaan H. Helfferich [a], Mahnaz Ghiasi [a], Johannes D. Meeldijk [a], Nienke J. Firet [c], Peter Ngene [a], Celso de Mello Donegá [b], Petra E. de Jongh [a,*]

[a] Inorganic Chemistry and Catalysis, Debye Institute for Nanomaterials Science, Utrecht University, Universiteitsweg 99, 3584 CG, Utrecht, the Netherlands
[b] Condensed Matter and Interfaces, Debye Institute for Nanomaterials Science, Utrecht University, Princetonplein 1, 3584 CC, Utrecht, the Netherlands
[c] Materials for Energy Conversion and Storage (MECS), Department of Chemical Engineering, Faculty of Applied Sciences, Delft University of Technology, van der Maasweg 9, 2629 HZ, Delft, the Netherlands

ARTICLE INFO

Keywords:
Copper sulfide
Nanoparticles
Carbon support
Sulfidation
CO_2 reduction
In situ X-ray absorption spectroscopy

ABSTRACT

The electrocatalytic reduction of CO_2 to produce sustainable fuels and chemicals is attracting great attention. Cu-based catalysts can lead to the production of a range of different molecules, and interestingly the product selectivity strongly depends on the preparation history, although it is not fully understood yet why. We report a novel strategy that allowed us to prepare Cu nanoparticle on carbon catalysts with similar morphologies, but prepared by in-situ reduction of either supported CuS, Cu_2S or CuO nanoparticles. For the first time the evolution of the Cu species was followed under CO_2 and H^+ reduction conditions using in-situ X-ray absorption spectroscopy. Excellent electrochemical contact between the Cu-based nanoparticles, the carbon support and the carbon-paper substrate was observed, resulting in metallic Cu as the predominant phase under typical electrochemical CO_2 reduction conditions. Even covering less than 4% of the H_2 producing carbon support with Cu-sulfide derived nanoparticles allowed to steer the selectivity to a maximum of 12% Faradaic efficiency for the production of formate. Clear differences between the catalysts derived from CuS, Cu_2S or CuO nanoparticles were observed, which was ascribed to the presence of residual sulfur in the catalysts.

1. Introduction

When using renewable electricity, the electrochemical reduction of carbon dioxide (CO_2) provides a promising route to produce chemicals and fuels in a sustainable manner. [1,2] The field of so called "solar fuels" has triggered the interest of many researchers, focusing on the development and understanding of electrocatalysts that can promote the electrochemical CO_2 reduction efficiently and with high selectivity to the targeted product.

The majority of the electrocatalysts studied for the reduction of CO_2 are based on transition metals. [3,4] As already described by Hori et al. in 1985, the catalytic performance of a catalyst highly depends on the metal used. [5] Metals such as gold [6,7], silver [8,9] and zinc produce mainly CO, whereas metals such as platinum, nickel and iron reduce only small amounts of CO_2, leading to H_2 as the main product formed via the competing hydrogen evolution reaction.

Copper electrodes are extensively studied and stand out because of their unique ability to produce hydrocarbons and oxygenates, which is ascribed to their intermediate binding strength for the CO intermediate. [1,5,10] Interestingly, Cu can lead to a range of different H^+ and CO_2 reduction products, and much work is done in the field to obtain a better understanding of the catalytic activity of Cu and the selectivity of Cu electrodes. For example, the use of oxide-derived Cu electrodes promotes the production of CO and COOH at low overpotentials, even though the electrodes are operating at potentials where all oxide should be reduced to metallic copper. [11,12] The exact explanation for the influence of the origin of the copper electrodes remains under debate, it might be attributed to the formation of specific surface structures of these oxide-derived electrodes [1], although also some oxygen remaining in the material might be a factor. [13]

* Corresponding author.
E-mail address: p.e.dejongh@uu.nl (P.E. de Jongh).
[1] Both authors contributed equally.

https://doi.org/10.1016/j.cattod.2020.09.020
Received 30 January 2020; Received in revised form 23 August 2020; Accepted 23 September 2020
Available online 1 October 2020

More recently, several experimental and theoretical studies have demonstrated that the addition of sulfur modifies the performance of Cu catalysts. [14–19] Even though copper sulfide is unstable under CO_2 and H^+ reduction conditions, most studies show that some sulfur remains on the catalyst after reaction. [14,15,17,18,20,21] Many of these studies observed an increased selectivity towards formate, that is often attributed to a change in the binding energy between the sulfur-containing catalyst and key intermediates in CO_2 reduction, such as *OCHO, *COOH and CO. [19] Besides an increased production of formate, other studies indicate an increased production of CO and/or CH_4 at low overpotentials when using sulfur derived Cu electrodes. [20,22] In addition, Zhuang et al. reported the production of ethanol, propanol and ethylene at intermediate overpotential (-0.95 V vs. RHE) using Cu_2S--derived nanoparticles. [21]

Inspired by these studies, in this work we investigated the catalytic performance and stability of copper sulfide ($Cu_{2-x}S$) derived nanoparticles supported on carbon for electrochemical CO_2 reduction. Copper sulfide consists of a family of chemical compounds with the formula $Cu_{2-x}S$, where x represents Cu vacancies. [23] $Cu_{2-x}S$ can thus exists in a variety of different compositions and crystal structures, which have different chemical and physical properties and possibly also different catalytic performance. Therefore, two $Cu_{2-x}S$ catalysts with different starting compositions were studied, namely covellite (CuS) and chalcocite (Cu_2S).

In thermal catalysts, techniques to prepare well-defined and uniformly distributed metal and metal oxide nanoparticles with tunable size have been well developed. [24] We explored a novel, two-step synthesis approach, building on known strategies for the preparation of supported CuO particles [25] followed by a liquid phase sulfidation. Carbon-supported CuS (CuS@C) or Cu_2S (Cu_2S@C) nanoparticles were synthesized by liquid phase sulfidation of carbon-supported CuO nanoparticles (CuO@C). This gave us a unique set of catalysts with very similar structural properties, that allowed us to investigate the influence of their chemical origin and of the presence of sulfur.

2. Experimental methods

2.1. Chemicals

XGnP500® graphene nanoplatelets (GNP) were purchased from XG Sciences. Copper(II) nitrate hydrate ($(CuNO_3)_2 \cdot 3\,H_2O$, 99 %), HNO_3 (70 %), thioacetamide (TAA, ≥99.0 %), Nafion® 117 solution, isopropanol (99.5 %) Potassium bicarbonate ($KHCO_3$, ≥99 %) and 1-dodecanethiol (DDT, ≥98 %) were purchased from Sigma Aldrich. Nafion™Membrane XL was obtained from Ion Power, GmbH and carbon paper (TGP-H-060) was purchased from Toray.

2.2. Synthesis of carbon supported CuO nanoparticles

Carbon supported CuO (CuO@C) nanoparticles were prepared via incipient wetness impregnation followed by drying and heat treatment. [24–27] 1 g of graphite nanoplatelets (GNP500) was dried under vacuum at 120 °C for 2 h and subsequently impregnated with an aqueous Cu $(NO_3)_2 \cdot 3\,H_2O$ solution in 0.1 M HNO_3. The volume used for impregnation corresponded to the total pore volume of the support, as determined with N_2-physisorption. A weight loading of 20 wt% Cu was used for all samples. After impregnation, the sample was left to dry overnight at room temperature under vacuum. Then the sample was transferred into a tubular reactor and heat treated at 230 °C for 2 h under a N_2 flow (200 mL/min) to decompose the $Cu(NO_3)_2$ into CuO nanoparticles.

2.3. Liquid-phase sulfidation of carbon-supported CuO nanoparticles

To obtain carbon supported CuS (CuS@C) nanoparticles, 400 mg of carbon supported CuO was dispersed into 40 mL demineralized water in a 100 mL roundbottom flask and heated to 120 °C. At a temperature of 90 °C, 10 mL of an aqueous thioacetamide solution was gradually added to the mixture, using a Cu:S molar ratio of 1:1.1. The mixture was left to reflux for 2 h at 120 °C. After 2 h, the mixture was left to cool down and subsequently washed with demineralized water and acetone using vacuum filtration. The samples were then dried under vacuum for 2 h.

To obtain carbon supported Cu_2S (Cu_2S@C) nanoparticles, 400 mg of carbon supported CuO was dispersed in 15 mL 1-dodecanethiol in a 100 mL roundbottom flask and subsequently heated to 200 °C. The mixture was left to react for 2 h and then cooled down to room temperature. The sample was washed using toluene and acetone and subsequently dried under vacuum at room temperature.

2.4. Working electrode preparation

The working electrodes were prepared by spraying the CuO@C, CuS@C and Cu_2S@C on a carbon paper substrate (Toray TGP-H-060). Prior to deposition of the catalyst, the carbon paper substrate was washed in ethanol by sonication for 30 min and subsequently rinsed with milliQ (MQ) water. Then, a catalyst ink was prepared by mixing 11 mg of carbon supported catalyst, 1120 μL isopropanol, 4470 μL MQ water and 44.4 μL Nafion solution. The ink was sonicated for 30 min in an ultrasonic bath to ensure good dispersion of the catalyst powder. Subsequently the ink was sprayed onto a round carbon paper electrode with a surface area of 4.9 cm^2 using an Iwata HP-BP HI Performace Plus airbrush. A catalyst loading of 0.2 mg/cm^2 (with 20 wt% Cu) was intended for all electrodes. The electrodes were dried overnight before electrochemical testing.

2.5. Characterization of catalyst and electrodes

The GNP500 support was characterized using N_2-physisorption performed with a Micromeritics TriStar instrument at a temperature of −196 °C. Prior to the measurements the powder was dried at 300 °C under N_2-flow for 16 h. The pore diameter was determined using the Barrett-Joyner-Halenda (BJH) method and the pore volume was determined at $p/p_0 = 0.995$.

Transmission electron microscopy (TEM) analysis was performed using a Thermo Fisher Scientific (formerly FEI) Tecnai12 microscope operating at 120 kV. The powder samples were suspended in ethanol and sonicated for 10 min. The suspension was then drop casted on a carbon coated 200 mesh copper TEM grid. Preparation of the TEM grids of the used catalyst was done by rubbing a TEM grid over the used electrode. Prior to this, the used electrodes were extensively rinsed with MQ water. TEM-EDX measurements were performed with a Thermo Fisher Scientific (formerly FEI) TalosF200X microscope, operating at 200 keV. For EDX measurements, gold TEM grids were used.

The electrodes before and after reaction were analyzed using scanning electron microscopy with energy dispersive X-ray spectroscopy (SEM-EDX) on a Thermo Fisher Scientific (formerly FEI) XL30SFEG instrument.

X-ray diffraction (XRD) measurements were done on a Bruker D2 Phaser, equipped with a Co Kα X-ray source with a wavelength of 1.79026 Å. The crystallite size of the copper sulfide nanoparticles was determined from the diffraction peak broadening using the Scherrer equation. [28]

2.6. Electrochemical measurements

A custom built, H-type electrochemical cell with two compartments separated by a Nafion membrane (Figure S1) was used for all electrochemical measurements. Each compartment of the electrochemical cell was filled with 11 mL electrolyte (0.5 M $KHCO_3$ or 0.5 M $KHCO_3$+0.5 M KCl). The anolyte was purged with Argon and the catholyte was purged with CO_2 at 10 mL/min. All electrochemical measurements were performed on an Autolab PGSTAT204 Potentiostat, with a Pt disk as counter electrode and a Ag/AgCl 3 M KCl reference electrode (Methrom). All

potentials were converted to the reversible hydrogen electrode (RHE) potential using the equation:

$$E\ (vs.\ RHE) = E\ (vs.\ Ag/AgCl) + 0.209 + 0.059\ x\ pH$$

The catalyst supported on the carbon paper electrode was placed on a glassy carbon electrode for extra support and held in place by O-rings, leaving an electrode area of 3.8 cm^2 in contact with the electrolyte solution. Prior to all measurements, either CO_2 or Argon was bubbled through the solution for 20 min.

Cyclic voltammetry was performed in a 0.5 M $KHCO_3$ electrolyte, a scanning rate of 10 mV/s and a constant Ar or CO_2 flow of 10 mL/min. The selectivity of the catalysts was determined using chronopotentiometry at different current densities for 5 h (liquid products) or 1 h (gaseous products). Gaseous products were analyzed by connecting the outlet of the cathode compartment to a Global Analysis Solutions Microcompact GC 4.0. The GC system was equipped with three channels: The first channel has a Rt-QBond (10 m*0.32 mm, Agilent) packed column and a FID detector for the detection of CH_4, C_2H_4 and C_2H_6, the second channel has Molecular Sieve 5A (10 m* 0.53 mm, Restek) packed column that separates small gaseous molecules such as CO, and CH_4. This channel has a FID detector with a methanizer to increase the detection sensitivity of CO. The third channel has a Carboxen 1010 (8m*0.32 mm, Agilent) packed column which separates H_2 and CO_2 with a TCD. High purity nitrogen (N_2; 99.999 %) was used as a carrier gas.

Liquid phase products were analyzed by analysis of the catholyte using a Varian HPLC equipped with a refractive index detector (RID) and a Bio-Rad Aminex HPX-87H column at 60 °C. 1 mM H_2SO_4 was used as the eluent with a flow rate of 0.55 mL/min. The retention time of formic acid was 15 min and the total analysis time was 20 min.

The Faradaic efficiency was calculated as:

$$FE(\%) = \frac{n_x\ x\ F\ x\ [moles\ of\ product\ x]}{Q} \times 100\%$$

In which n_x is the number of electrons needed to produce x (product) from CO_2 molecules and F is the Faradaic constant (96 485 s·A/mol).

For gaseous products (x = H_2, CO, CH_4, C_2H_4, or C_2H_6), the moles of product were determined via:

$$moles\ of\ product = \frac{C_X \times q \times p}{RT}$$

in which C_x is the volumetric concentration of product x in ppm extracted from the GC calibration curve, q is the gas flow rate, p is the pressure, R is the ideal gas constant (8.314 $m^3 \cdot Pa \cdot K^{-1} \cdot mol^{-1}$, T is the temperature, n_x is the number of electrons needed to produce x (product) from CO_2 molecules and F is the Faradaic constant (96 485 s·A/mol).

For liquid phase products (x = formate), the moles of product formed was determined via:

$$moles\ of\ product = \frac{C_X \times V_{catholyte}}{1000 \times M_w}$$

in which C_x is the volumetric concentration of product x in ppm extracted from the HPLC calibration curve, $V_{catholyte}$ is the volume of the catholyte (L) and M_w the molar weight of product x (g/mol).

2.7. XAS measurements

X-ray absorption measurements were performed at the Dutch-Belgian beamline DUBBLE, 26A at the European Synchrotron Radiation Facility (ESRF) in Grenoble, France. Spectra were recorded at the Copper K-edge (8978.9 eV). Reference spectra of CuS@C, Cu_2S@C and Cu foil were recorded in transmission mode. The Athena XAS data processing software was used for the analysis of data.

For the in-situ XAS measurements, an electrochemical cell made by TU Delft was used (Figure S2). [29] All in-situ experiments were performed in fluorescence mode, with an angle of 45° between the incoming X-rays and the sample. The time to acquire a spectrum was about 4.5 min and 2–5 scans were recorded at each potential. A CO_2-saturated 0.1 M $KHCO_3$ electrolyte was flown through the cell with a flowrate of 2 mL/min using a peristaltic pump. The $Cu_{2-x}S$@C electrodes were used as working electrode, a coiled platinum wire as counter electrode and a Ag/AgCl 3M KCl electrode as reference electrode. A BioLogic SP-240 potentiostat was used for all in-situ XAS experiments.

3. Results and discussion

3.1. Structural properties of the catalyst and electrodes

Supported CuS and Cu_2S catalysts were prepared via a novel, two-step synthesis route, in which carbon supported CuO nanoparticles (CuO@C) were converted into carbon supported CuS (CuS@C) or Cu_2S (Cu_2S@C) nanoparticles. This approach was chosen in order to investigate whether the nanoparticle size of the CuO@C sample could be maintained in the CuS@C and Cu_2S@C samples. Fig. 1 shows the X-ray diffractograms of CuO@C, CuS@C, Cu_2S@C and of bare carbon as a reference. For all four samples, diffraction lines are observed at 30.6° and 64.1°, which can be ascribed to the crystalline graphite support, which clearly was not damaged by the treatments. The CuO@C sample shows additional diffraction lines at 41.5°, 45.3° and 57.0°, which can be indexed with the monoclinic structure of CuO (PDF-01-070-6831 (ICDD, 2019) [30]). Upon sulfidation using thioacetamide, the diffraction pattern shows clear diffraction lines at 34.1°, 37.1°, 38.3° and 56.3°, which is consistent with the hexagonal CuS covellite structure (PDF-00-006-0464 (ICDD, 2019) [30]). The formation of metal sulfides using TAA has been described before and two different mechanisms are proposed [31–33]. CuS can be formed in a direct reaction, via the formation and subsequent decomposition of Cu-TAA complexes, or via a hydrolysis reaction, where the hydrolysis of TAA yields H_2S and H_2S subsequently reacts with Cu^{2+} (either dissolved or in CuO nanoparticles) to form CuS.

Upon sulfidation using 1-dodecanethiol, the reflections at 44.0°, 54.3° and 57.2° demonstrate the presence of hexagonal Cu_2S chalcocite (PDF-00-053-0522 (ICDD, 2019) [30]). The formation of the supported Cu_2S nanoparticles from Cu^{2+} and DDT likely proceeded via the

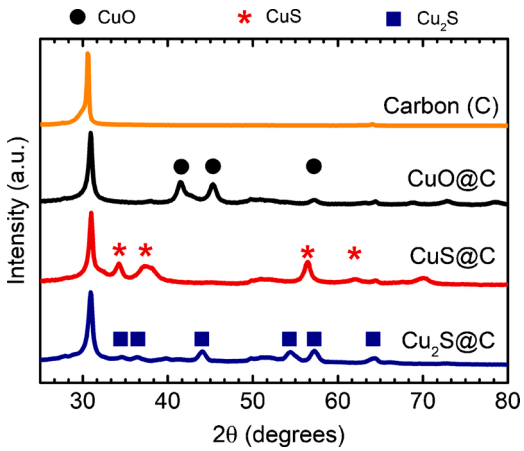

Fig. 1. X-ray diffractograms of the bare GNP-500 carbon support (orange) and of the CuO@C (black), CuS@C (red) and Cu_2S@C (blue) nanoparticles on this carbon support. All samples have a loading of 20 wt% Cu. The symbols above the diffractograms represent reflections of CuO (black dot), CuS (red asterisk) and Cu_2S (blue square), obtained from the PDF reference cards PDF-01-070-6831 (ICDD, 2019), PDF-00-006-0464 (ICDD, 2019) and PDF-00-053-0522 (ICDD, 2019), respectively. For interpretation of the references to colour in this figure legend, the reader is referred to the web version of this article.[29]

formation of Cu-thiolate complexes, which were subsequently decomposed by thermal cleavage of the C–S bond, resulting in Cu-S monomers for nucleation and growth of Cu_2S nanoparticles.

For both the CuS@C and Cu_2S@C, no residual CuO reflections are observed, hence complete conversion of CuO to either CuS or Cu_2S was achieved. The relative broad peaks in the CuO@C, CuS@C and Cu_2S@C samples prove the presence of nanocrystallites and the absence of macrocrystalline material. The Scherrer equation was used to determine the crystallite size of the particles, resulting in crystallite sizes of 13, 14 and 12 nm for the CuO@C, CuS@C and Cu_2S@C samples, respectively.

Fig. 2 shows the transmission electron microscopy (TEM) images of the supported nanoparticles and the corresponding particle size histograms. Both the CuO@C and the Cu_2S@C samples show spherical particles with a particle size of 9 ± 3 nm for CuO and 17 ± 1 nm for Cu_2S. The supported CuS nanoparticles have a larger size of 25 ± 13 nm, with a few particles larger than 30 nm (Figure S3) and a platelet-like morphology (Fig. 2b). The CuO@C nanoparticles can thus be successfully converted to nanoparticles of either CuS@C or Cu_2S@C. However, especially for CuS@C significant particle growth is observed upon sulfidation. The increase in particle size upon sulfidation is likely caused by (partial) dissolution of the CuO@C nanoparticles caused by the high temperatures used during sulfidation (120 °C for CuS@C and 200 °C Cu_2S@C). The dissolved Cu^{2+} ions can react with either TAA or DDT and redeposit as CuS or Cu_2S, respectively, via the mechanisms described above.

The working electrodes CuO@C, CuS@C or Cu_2S@C were prepared by spraying an ink containing the catalyst powder onto carbon paper substrates. Fig. 3 shows representative scanning electron microscopy (SEM) images of the bare carbon paper substrate and of the Cu_2S@C nanoparticles sprayed onto the carbon paper substrate, illustrating the distribution over and adherence of the Cu_2S@C to the carbon paper substrate. CuS@C was also well distributed over the carbon paper (Figure S4).

3.2. Electrochemical characterization of the catalyst under eCO_2R reaction conditions

Fig. 4 shows the cyclic voltammograms of CuS@C and Cu_2S@C in a 0.5 M $KHCO_3$ electrolyte (pH = 7.1) under argon flow, obtained with a

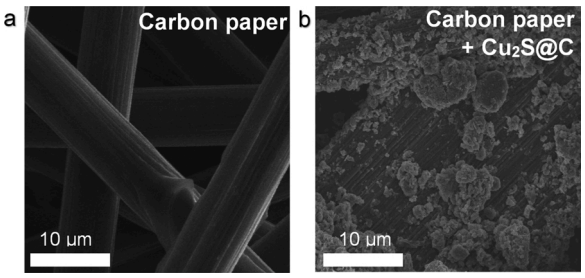

Fig. 3. SEM images of the carbon paper substrate a) without any catalyst and b) with Cu_2S@C deposited on the carbon fibers by spraying.

scan rate of 10 mV/sec. For each sample, the first 5 cycles are shown. For CuS@C (Fig. 4a), two reduction peaks are observed in the first cathodic scan at potentials of around -0.1 V and -0.5 V, with onsets around -0.0 V and -0.4 V vs. RHE, respectively. Figure S5 shows the Pourbaix diagram of an aqueous Cu-S system at 25 °C with Cu and S concentrations of 1 M. The diagram shows that under these conditions, CuS is not thermodynamically stable at potentials more negative than -0.4 V vs. SHE (0.0 V vs. RHE) in aqueous solutions at pH 7, and can be reduced, via several copper rich $Cu_{2-x}S$ phases, to metallic Cu. Relating this to the reduction peaks observed in the voltammogram of CuS@C, the first reduction peak can be attributed to a reduction of the CuS nanoparticles to more copper-rich copper sulfide phases, such as djurleite($Cu_{1.94}S$) or chalcocite (Cu_2S). The second reduction peak can then be attributed to the reduction of the remaining $Cu_{2-x}S$ phase to metallic Cu.

The Cu_2S@C sample (Fig. 4b) also shows a reduction peak around -0.5 V vs. RHE, with an onset around -0.4 V vs. RHE, which corresponds to a reduction of the $Cu_{2-x}S$ nanoparticles to metallic Cu. In addition, a reduction peak is observed around a potential of -0.4 V, with an onset at -0.2 V. This reduction likely originates from a reduction of a more copper deficient $Cu_{2-x}S$ phase or some CuO, which was formed during the storage of the electrode in air prior to the measurements. Figure S6 shows the voltammogram of the CuO@C sample, showing two reduction peaks with onsets above 0 V vs. RHE and around -0.2 V vs. RHE in the first cathodic scan. These reduction peaks correspond to the ready reduction of CuO to Cu_2O and subsequently metallic Cu. [34]

The CVs thus show that CuS@C and Cu_2S@C are reduced to metallic

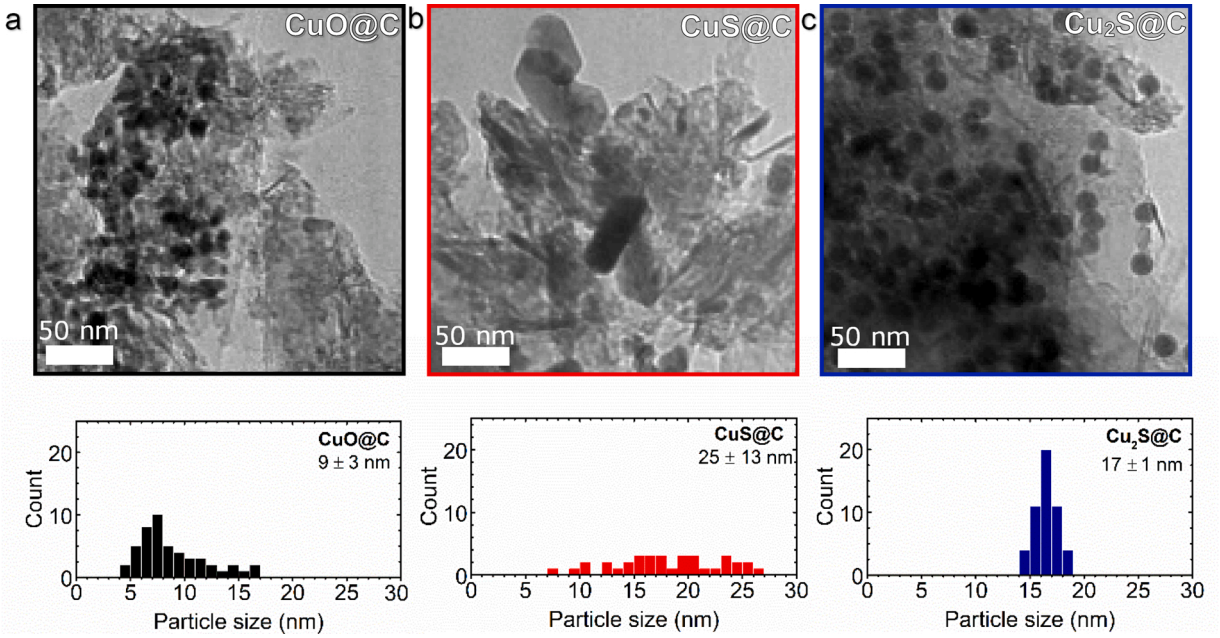

Fig. 2. TEM images of a) CuO@C, b) CuS@C and c) Cu_2S@C nanoparticles and corresponding particle size histograms, indicating an average particle size of 9 ± 3 nm, 25 ± 13 nm and 17 ± 1 nm, respectively.

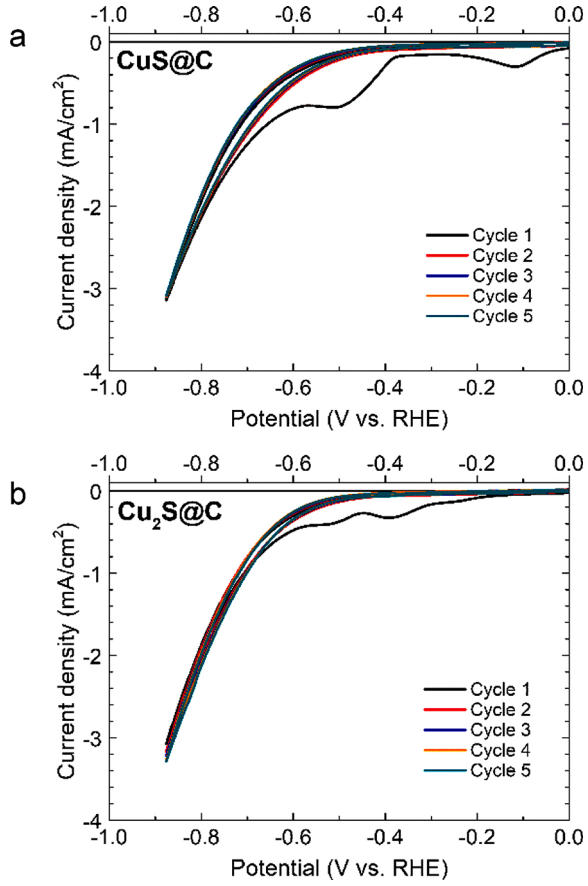

Fig. 4. Voltammograms of a) CuS@C and b) Cu_2S@C in a Ar-saturated 0.5 M $KHCO_3$ solution (pH = 7.1). A scan rate of 10 mV/s was used for all measurements. The reduction of the Cu-based nanoparticles is clearly visible in the first cathodic scan.

Cu when scanning to potentials more negative than -0.4 V vs. RHE. However, no oxidation peaks are observed in the anodic cycles of the CVs (Fig. 4a,b), indicating the reduced phases do not oxidize back to the original CuS or Cu_2S phase in this potential range. During reduction, the sulfur will likely react with protons from solution to form $SH^-_{(aq)}$ and $H_2S_{(g)}$. [15] The gaseous H_2S will escape from the cell, explaining the irreversibility of the reduction of CuS and Cu_2S.

X-ray absorption spectroscopy (XAS) was employed to probe the copper phases under operando reaction conditions. In-situ techniques are invaluable as the characterization of catalysts after reaction is challenging due to the limited amount of catalyst used in reactions. In addition, the catalyst is often highly susceptible to changes when a potential is no longer applied, and the catalyst is removed from the electrolyte solution (e.g. oxidation). XAS is a very suitable technique for in-situ studies of electrocatalysts, as X-rays can easily penetrate through air and water due to their high energy. [35–37]

Fig. 5 shows the ex-situ XAS spectra of the CuS@C and Cu_2S@C samples (dotted lines) and the in-situ XAS spectra of these samples (solid lines). The conditions under which the samples were measured are different. The ex-situ spectra were recorded on pellets of the as-synthesized powder samples. In contrast, the in-situ spectra shown in Fig. 5a are of the CuS@C and Cu_2S@C powders, deposited on the carbon paper substrate, in contact with a CO_2 saturated 0.1 M $KHCO_3$ electrolyte (pH = 6.8), without applying a potential. However, for both CuS@C and Cu_2S@C, the in-situ spectrum shows the same features as the corresponding sample measured under ex-situ conditions. This demonstrates that the CuS@C and Cu_2S@C were stable upon deposition of the catalyst powder on the carbon paper substrate and subsequent contact with the CO_2 saturated electrolyte, and hence validates the in-situ measurements.

Subsequently, the CuS@C and Cu_2S@C samples were analyzed under CO_2 and H^+ reduction conditions. Fig. 6a shows the in-situ XAS spectra of the CuS@C sample upon applying negative potentials of -0.9 V, -1.2 V and 1.6 V vs. RHE. Additional spectra of the sample at potentials of -0.05 V, -0.25 V and -0.6 V vs. RHE are shown in Figure S7. Up to a potential of -0.6 V, no clear changes are observed in the XAS spectra when compared to the spectrum of the ex situ CuS@C sample (Figure S7). Upon applying potentials more negative than -0.9 V vs. RHE, the spectra show clear changes, features start to appear at energies of 9025 eV and 9070 eV. When going to more negative potentials, such as -1.2 V and -1.6 V vs. RHE, these features become even more pronounced. As is shown by the ex-situ XAS pattern of the Cu foil, the peaks at 9025 eV and 9070 eV are characteristic for metallic Cu. Although it is difficult to distinguish if the reduction occurs via any intermediate copper-rich $Cu_{2-x}S$ phases, the in-situ XAS data thus clearly show the reduction of the CuS nanoparticles to metallic Cu under reaction conditions.

Fig. 6b shows the in-situ XAS spectra of the Cu_2S@C sample under reaction conditions. Whereas for the CuS@C sample at -0.9 V vs. RHE the spectrum only showed minor changes compared to the as-prepared CuS@C spectrum, the spectrum of the Cu_2S@C sample at -0.9 V already clearly resembles the metallic Cu reference. This indicates a ready reduction of the Cu_2S nanoparticles to metallic Cu.

This technique thus allowed us to elucidate the chemical phase of the catalyst under electrochemical CO_2 reduction conditions. For both samples, the potential at which a reduction to Cu is observed by XAS (-0.9 V) is more negative than the potential of -0.5 V vs. RHE at which the reduction peak was observed in the CVs (Fig. 4b,c). This is likely caused by the different experimental conditions used in the two experiments, such as the different cell geometries (see Figure S1, S2) leading to differences in ohmic resistance. In addition, an electrolyte

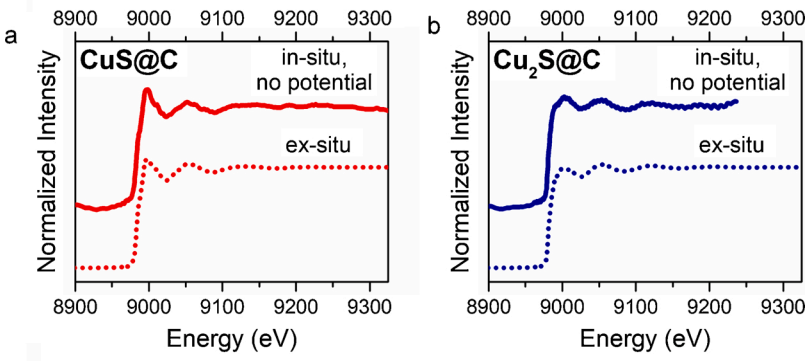

Fig. 5. a) Normalized XAS spectra of a) Cus@C and b) Cu_2S@C, comparing an ex-situ measurement (dotted lines) with that of the sample as electrode in the electrochemical cell, without applying a potential (solid lines).

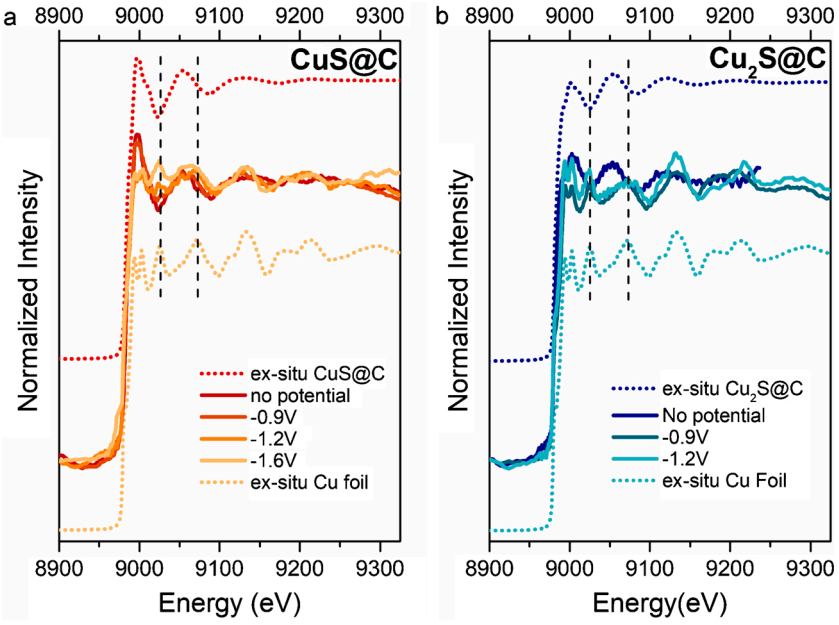

Fig. 6. a) Normalized XAS spectra of CuS@C measured in-situ during electrochemical CO_2 reduction at different potentials (solid lines), compared to ex-situ reference spectra of CuS@C (dotted, red line) and Cu foil (dotted, orange line). Upon applying a more negative potential, the spectra resemble the Cu foil reference, indicating a reduction of the CuS to Cu. b). Normalized XAS spectra of Cu_2S@C measured in-situ during CO_2 reduction at different potentials (solid lines), compared to ex-situ reference spectra of Cu_2S@C (dotted, dark blue line) and Cu foil (dotted, light blue line). Upon applying a more negative potential, the spectra resemble the Cu foil reference, indicating a reduction of the Cu_2S to Cu. For interpretation of the references to colour in this figure legend, the reader is referred to the web version of this article.

concentration of 0.1 M $KHCO_3$ was used during the in-situ XAS experiments, as compared to a concentration of 0.5 M $KHCO_3$ and the resulting lower conductivity and pH is expected to shift the reduction to slightly more negative potentials. Therefore additional CV measurements were performed in the XAS cell. The reduction peaks of the reduction of the CuS@C and Cu_2S@C sample to metallic Cu are clearly visible at -0.63 V vs. RHE for both samples (supporting information, Figure S8). When comparing these values to the position of the reduction peaks in the H-type cell (supporting information, Table S1), we see that the reduction peak of the reduction of $Cu_{2-x}S$ to metallic Cu is indeed shifted to more negative potentials when using the XAS cell.

Most importantly, XAS is a bulk technique and from the fact that the spectra at potentials more negative than -0.9 V correspond to metallic Cu, with very little or none of the original ex-situ spectrum remaining, it can be concluded that the vast majority of the nanoparticles is electrochemically active, and in good electrochemical contact with the carbon support and carbon-paper substrate as well as with the electrolyte solution. This is the first time that the chemical phases of CuS@C- and Cu_2S@C-derived catalysts were followed in-situ under CO_2 and H^+ reduction conditions, giving valuable insight in the active catalyst phase and on the electrochemical contact between the nanoparticles and support material.

3.3. Electrochemical CO_2 reduction

The product selectivity of the CuS@C and Cu_2S@C derived catalysts in electrochemical CO_2 reduction were compared to that of the CuO@C derived catalyst. For all three catalysts, the main CO_2 reduction product formed was formate. Table 1 shows the amount of formate produced for all three catalysts and a carbon reference and two sulfidized carbon reference, treated with either TAA or DDT, obtained from chronopotentiometry (CP) for 5 h in a 0.5 M KCl + 0.5 M $KHCO_3$ electrolyte saturated with CO_2 at current densities of -1.5, -3.0 and -4.5 mA/cm^2. Corresponding bar charts are shown in Figure S9. Here, the KCl was added as supporting electrolyte to increase the conductivity of the electrolyte and minimize ohmic resistances. Figure S10 shows the potentials over time obtained during the 5 h CP experiments.

When a current density of -1.5 mA/cm^2 was applied, formate was produced with yields of 9, 13 and 3 μmol/hr for the CuS@C-, Cu_2S@C- and CuO@C-derived catalysts, respectively. As the the CuO@C-derived catalyst showed a similar production of formate (3 μmol/hr) to the bare carbon support and the two sulfidized carbon supports (3 μmol/hr, 1 μmol/hr and 5 μmol/hr for C, C-TAA and C-DDT, respectively), the production of formate on this catalyst is considerably less. The production of formate on the CuS@C- and Cu_2S@-derived catalysts is however significantly higher, showing that the production of formate is clearly promoted on the sulfide derived catalysts when compared to the oxide derived catalyst and the carbon support. In addition, more formate is produced by the Cu_2S@C-derived catalyst than by the CuS@C-derived catalyst. This indicates that, even though both CuS@C and Cu_2S@C reduce to metallic Cu under reaction conditions, there is a difference between the two Cu-sulfide derived catalysts depending on whether they originate from CuS@C or Cu_2S@C. When applying more negative potentials, the formate production also on the oxide-derived catalyst

Table 1
The amount of formate produced and Faradaic efficiency of formate during CO_2 reduction using CuO@C, CuS@C and Cu_2S@C, a carbon reference and two sulfidized carbon references, treated with either TAA or DDT, at different currents applied. The data is obtained by CP for 5 h with currents of -1.5, -3 and -4.5 mA/cm^2, performed in a 0.5 M KCl +0.5 M $KHCO_3$ electrolyte saturated with CO_2 (pH 7.5). The average potentials over 5 h of CP are also shown (with standard deviation).

Applied current density (mA/cm$^2_{geometrical}$)	Sample	Formate Production (μmol/hr)	Faradaic Efficiency Formate (%)	Resulting Potential (V vs. RHE)
−1.5	CuS@C	9	8	−0.77 ± 0.02
	Cu_2S@C	13	12	−0.78 ± 0.02
	CuO@C	3	3	−0.66 ± 0.04
	C	3	3	−0.82 ± 0.02
	C-TAA	1	1	−0.93 ± 0.01
	C-DDT	5	4	−0.96 ± 0.05
−3	CuS@C	14	7	−0.90 ± 0.08
	Cu_2S@C	21	10	−0.76 ± 0.01
	CuO@C	16	8	−0.88 ± 0.10
	C	4	2	−0.96 ± 0.01
	C-TAA	3	1	−1.13 ± 0.06
	C-DDT	4	2	−1.00 ± 0.02
−4.5	CuS@C	11	3	−1.05 ± 0.05
	Cu_2S@C	12	4	−0.87 ± 0.03
	CuO@C	19	6	−0.91 ± 0.02
	C	6	2	−1.65 ± 0.03
	C-TAA	4	1	−1.20 ± 0.07
	C-DDT	4	1	−1.06 ± 0.03

increases, making the differences less pronounced, although in all cases the Cu_2S@C-derived catalyst produces more formate than the CuS@C-derived catalyst.

Besides formate, only small amounts of CO were produced with Faradaic efficiencies between 0–1.3 % (Table S2, Figure S11). The differences between the measured CO concentrations on the different catalysts were close to the experimental error. No other CO_2 reduction products were found in the liquid or gaseous phase and hence the rest of the current led to the production of H_2. The production of H_2 readily occurred on the bare carbon reference sample. In fact, the loading with Cu-based nanoparticles corresponds to a surface coverage of less than 4% of the carbon support (see Support Information for calculations). It is hence amazing that CO_2 reduction products with Faradaic efficiencies ranging from 3 to 12% can be obtained with such a low coverage of the carbon surface, which so readily produced H_2 instead. This means that the Cu-based nanoparticles clearly introduce a strong preference for CO_2 rather than H^+ reduction.

The enhanced selectivity for formate on the sulfide derived catalysts at current densities of -1.5 mA/cm^2 is consistent with previous studies and can be explained by the different pathways possible for CO_2 reduction. [14,15,17,18] Norskov et al. proposed that the reduction of CO_2 to HCOO- occurs via a *OCHO intermediate, which is further reduced to formate (HCOO-). [38] On the other hand, other studies suggest the formation of formate occurs via a direct reaction of physisorbed CO_2 with adsorbed H^+. [18,39] In both mechanisms, CO and further reduced products are formed via a so-called CO pathway, in which CO_2 is reduced to *COOH, which can be further reduced to *CO, which in turn can desorb or be further reduced to various hydrocarbons and alcohols. Although no distinction can be made between the two mechanism to form formate, the increased selectivity for formate observed for the sulfide derived catalysts at a current densities of -1.5 mA/cm^2 suggests that the HCOO- pathway is favored over the CO pathway. Which pathway is preferred highly depends on the binding strength of important intermediates such as CO on the catalyst, suggesting that the binding affinity for the CO_2 reduction intermediates is different on the sulfide-derived catalysts than on the oxide-derived catalyst. Nevertheless, elucidation of the exact role of sulfur on the CO_2 reduction mechanism will require additional studies.

3.4. Structure of catalyst after reaction

The increased formation of formate on Cu_2S@C-derived catalyst when compared to CuS@C-derived catalyst suggests a difference in the chemical composition between the two. Hence, additional characterization of the catalysts after reaction was performed. After being used in the CO_2 and H^+ reduction for 5 h at -3 mA/cm^2 in 0.5 M KCl + 0.5 M $KHCO_3$, the CuO@C-, CuS@C- and Cu_2S@C-derived catalysts were analyzed to see if any changes occurred upon reaction. Fig. 7 shows TEM images of the CuO@C-, CuS@C- and Cu_2S@C-derived catalysts after being employed in the CO_2 reduction reaction. For CuO@C, the particle size increased from 9 ± 3 nm to 33 ± 14 nm. For the CuS@C-derived catalyst, no significant change in particle size is observed, whereas for the Cu_2S@C-derived catalyst, the particle size decreased from 17 ± 1 nm to 6 ± 2 nm upon reaction. Upon reaction, the CuO@C- and CuS@C-derived catalysts thus have a fairly similar particle size distribution, while the Cu_2S@C-derived catalyst has smaller and more monodisperse particles. This difference in particle size could play a role in the different catalytic behavior discussed in section 3.3..._[40,41] The larger size of the CuS@C-derived catalyst when compared to the Cu_2S@C-derived catalyst can possibly explain the lower selectivity to formate for the CuS@C-derived catalyst, as the larger CuS-derived particles have a lower electrochemically active surface area.

In addition, TEM-EDX measurements were performed to analyze the presence of sulfur in the catalysts after reaction. The measurements showed remaining sulfur in the samples after reaction, where copper to sulfur ratios of 3:1 and 6:1 were found for the CuS@C- and Cu_2S@C-derived catalyst, respectively (Table S3). This was much higher than the sulfur content detected in the CuO@C sample, with a Cu:S ratio of 32:1. This sample was used as a reference for the base sulfur content, as the Nafion binder used in the electrode preparation contains some sulfur as well. A small amount of sulfur, as well as K and Cl, (Figure S13) can also be ascribed to incomplete removal of the electrolyte. Although precise quantification is thus not straight-forward, it is clear that sulfur content is higher for the CuS@C derived catalyst than for Cu_2S@C-derived catalyst, which can be explained by the higher initial sulfur content of CuS@C, and for both sulfide derived catalysts much higher than for the oxide derived catalyst. Also the difference in sulfur content likely influences the product selectivities observed for the two sulfide-derived catalysts.

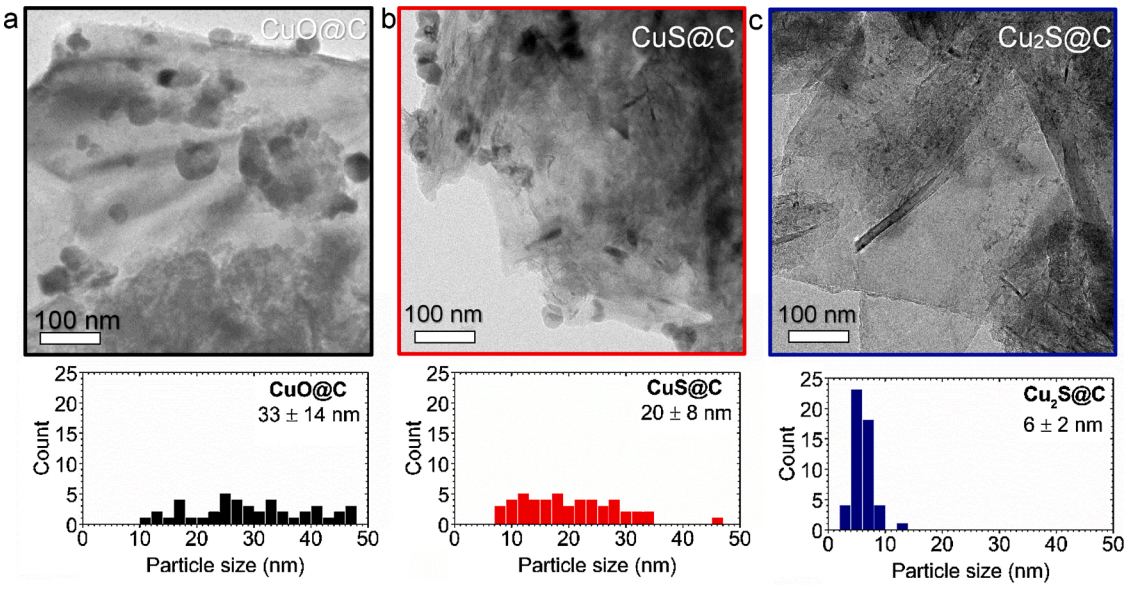

Fig. 7. TEM figures of the a) CuO@C-, b) CuS@C-, and c) Cu_2S@C-derived catalysts after 5 h of CO_2 and H^+ reduction at -3 mA/cm^2 in 0.5 M KCl +0.5 M $KHCO_3$. The lower panels show corresponding particle size histograms. For CuO@C, a few particles larger than 50 nm were also observed (Figure S12).

4. Conclusions

In summary, carbon-supported, $Cu_{2-x}S$ derived nanoparticles were studied for electrochemical CO_2 reduction in aqueous media. First, CuS@C and Cu_2S@C nanoparticles were successfully prepared via a liquid phase sulfidation of CuO@C nanoparticles. Subsequently the catalysts were deposited on carbon paper electrode substrates. Upon electrochemical CO_2 reduction, CuS@C and Cu_2S@C nanoparticles undergo a reduction to metallic Cu, as was verified by both CV and in-situ XAS experiments. EDX measurements showed that some residual sulfur is left in both catalysts. The selectivity of the CuS@C- and Cu_2S@C-derived catalysts was tested and compared to that of a CuO@C-derived catalyst. On all three catalysts, formate was produced as the main CO_2 reduction product, next to H_2 mainly produced by the carbon support. At low current densities, the selectivity towards the production of formate was enhanced for the CuS@C- and Cu_2S@C-derived catalysts when compared to the CuO@C derived catalyst. It is remarkable that with less than 4% carbon surface coverage, a maximum of 12% Faradaic efficiency overall selectivity to formate was achieved, showing the effectiveness of Cu-sulfide derived catalysts to steer the selectivity to formate. In addition, the two Cu-sulfide derived catalysts showed clear differences in formate production, indicating the initial Cu-sulfide phase influences the product selectivity.

CRediT authorship contribution statement

Christina H.M. van Oversteeg: Investigation, Formal analysis, Writing - original draft, Writing - review & editing. **Marisol Tapia Rosales:** Investigation, Formal analysis, Writing - review & editing. **Kristiaan H. Helfferich:** Investigation, Writing - review & editing. **Mahnaz Ghiasi:** Formal analysis. **Johannes D. Meeldijk:** Investigation, Formal analysis. **Nienke J. Firet:** Investigation. **Peter Ngene:** Investigation, Writing - review & editing, Supervision. **Celso de Mello Donegá:** Writing - review & editing, Supervision. **Petra E. de Jongh:** Writing - review & editing, Supervision.

Declaration of Competing Interest

The authors report no declarations of interest.

Acknowledgements

This work was supported by the Netherlands Center for Multiscale Catalytic Energy Conversion (MCEC), a NWO Gravitation program funded by the Ministry of Education, Culture and Science of the government of the Netherlands, and by the European Research Council, project number ERC-2014-CoG 648991. MTR acknowledges the NWO-EleReCet project, which is part of the Solar-to-Products program funded by the Dutch Research Council (NWO), for funding. We are grateful to Alessandro Longo at the ESRF for providing assistance in using beamline 26 – The Dutch-Belgian Beam Line (DUBBLE). Fei Chang is thanked for his help during the XAS beamtime. Sneh Sameer is thanked for his help on the electrochemical cell design. Kai Han, Francesco Mattarozzi and Jan Willem de Rijk are acknowledged for useful discussions on the electrochemical set-up and measurements.

Appendix A. Supplementary data

Supplementary material related to this article can be found, in the online version, at doi:https://doi.org/10.1016/j.cattod.2020.09.020.

References

[1] S. Nitopi, E. Bertheussen, S.B. Scott, X. Liu, A.K. Engstfeld, S. Horch, B. Seger, I.E. L. Stephens, K. Chan, C. Hahn, J.K. Nørskov, T.F. Jaramillo, I. Chorkendorff, Progress and perspectives of electrochemical CO2 reduction on copper in aqueous electrolyte, Chem. Rev. 119 (2019) 7610–7672, https://doi.org/10.1021/acs.chemrev.8b00705.

[2] A.M. Appel, J.E. Bercaw, A.B. Bocarsly, H. Dobbek, D.L. Dubois, M. Dupuis, J. G. Ferry, E. Fujita, R. Hille, P.J.A. Kenis, C.A. Kerfeld, R.H. Morris, C.H.F. Peden, A. R. Portis, S.W. Ragsdale, T.B. Rauchfuss, J.N.H. Reek, L.C. Seefeldt, R.K. Thauer, G. L. Waldrop, Frontiers, opportunities, and challenges in biochemical and chemical catalysis of CO2 fixation, Chem. Rev. 113 (2013) 6621–6658, https://doi.org/10.1021/cr300463y.

[3] Y.Y. Birdja, E. Pérez-Gallent, M.C. Figueiredo, A.J. Göttle, F. Calle-Vallejo, M.T. M. Koper, Advances and challenges in understanding the electrocatalytic conversion of carbon dioxide to fuels, Nat. Energy 4 (2019) 732–745, https://doi.org/10.1038/s41560-019-0450-y.

[4] Y. Hori, H. Wakebe, T. Tsukamoto, O. Koga, Electrocatalytic process of CO selectivity in electrochemical reduction of CO2 at metal electrodes in aqueous media, Electrochim. Acta 39 (1994) 1833–1839, https://doi.org/10.1016/0013-4686(94)85172-7.

[5] Y. Hori, K. Kikuchi, S. Suzuki, Production of Co and Ch 4 in electrochemical reduction of Co 2 At metal electrodes in aqueous hydrogencarbonate solution, Chem. Lett. 14 (1985) 1695–1698, https://doi.org/10.1246/cl.1985.1695.

[6] E.R. Cave, J.H. Montoya, K.P. Kuhl, D.N. Abram, T. Hatsukade, C. Shi, C. Hahn, J. K. Nørskov, T.F. Jaramillo, Electrochemical CO $_2$ reduction on Au surfaces: mechanistic aspects regarding the formation of major and minor products, Phys. Chem. Chem. Phys. 19 (2017) 15856–15863, https://doi.org/10.1039/C7CP02855E.

[7] Y. Chen, C.W. Li, M.W. Kanan, Aqueous CO $_2$ reduction at very low overpotential on oxide-derived Au nanoparticles, J. Am. Chem. Soc. 134 (2012) 19969–19972, https://doi.org/10.1021/ja309317u.

[8] T. Hatsukade, K.P. Kuhl, E.R. Cave, D.N. Abram, T.F. Jaramillo, Insights into the electrocatalytic reduction of CO $_2$ on metallic silver surfaces, Phys. Chem. Chem. Phys. 16 (2014) 13814–13819, https://doi.org/10.1039/C4CP00692E.

[9] Y.T. Guntern, J.R. Pankhurst, J. Vávra, M. Mensi, V. Mantella, P. Schouwink, R. Buonsanti, Nanocrystal/metal–organic framework hybrids as electrocatalytic platforms for CO2 conversion, Angew. Chemie - Int. Ed. 58 (2019) 12632–12639, https://doi.org/10.1002/anie.201905172.

[10] R. Kortlever, J. Shen, K.J.P. Schouten, F. Calle-Vallejo, M.T.M. Koper, Catalysts and reaction pathways for the electrochemical reduction of carbon dioxide, J. Phys. Chem. Lett. 6 (2015) 4073–4082, https://doi.org/10.1021/acs.jpclett.5b01559.

[11] R. Kas, R. Kortlever, A. Milbrat, M.T.M. Koper, G. Mul, J. Baltrusaitis, Electrochemical CO2 reduction on Cu2O-derived copper nanoparticles: controlling the catalytic selectivity of hydrocarbons, Phys. Chem. Chem. Phys. 16 (2014) 12194–12201, https://doi.org/10.1039/c4cp01520g.

[12] Y. Lum, B. Yue, P. Lobaccaro, A.T. Bell, J.W. Ager, Optimizing C-C coupling on oxide-derived copper catalysts for electrochemical CO2 reduction, J. Phys. Chem. C. 121 (2017) 14191–14203, https://doi.org/10.1021/acs.jpcc.7b03673.

[13] F. Cavalca, R. Ferragut, S. Aghion, A. Eilert, O. Diaz-Morales, C. Liu, A.L. Koh, T. W. Hansen, L.G.M. Pettersson, A. Nilsson, Nature and distribution of stable subsurface oxygen in copper electrodes during electrochemical CO2 reduction, J. Phys. Chem. C 121 (2017) 31, https://doi.org/10.1021/acs.jpcc.7b08278.

[14] Y. Deng, Y. Huang, D. Ren, A.D. Handoko, Z.W. Seh, P. Hirunsit, B.S. Yeo, On the role of sulfur for the selective electrochemical reduction of CO2 to formate on CuSx catalysts, ACS Appl. Mater. Interfaces 10 (2018) 28572–28581, https://doi.org/10.1021/acsami.8b08428.

[15] T. Shinagawa, G.O. Larrazábal, A.J. Martín, F. Krumeich, J. Pérez-Ramírez, Sulfur-modified copper catalysts for the electrochemical reduction of carbon dioxide to formate, ACS Catal. 8 (2018) 837–844, https://doi.org/10.1021/acscatal.7b03161.

[16] Q.G. Zhu, X.F. Sun, X.C. Kang, J. Ma, Q.L. Qian, B.X. Han, Cu2S on cu foam as highly efficient Electrocatalyst for Reduction of Co2 to formic acid, Wuli Huaxue Xuebao/ Acta Phys. - Chim. Sin. 32 (2016) 261–266, https://doi.org/10.3866/PKU.WHXB201512101.

[17] Y. Huang, Y. Deng, A.D. Handoko, G.K.L. Goh, B.S. Yeo, Rational design of sulfur-doped copper catalysts for the selective electroreduction of carbon dioxide to formate, ChemSusChem. 11 (2018) 320–326, https://doi.org/10.1002/cssc.201701314.

[18] K.R. Phillips, Y. Katayama, J. Hwang, Y. Shao-Horn, Sulfide-derived copper for electrochemical conversion of CO 2 to formic acid, J. Phys. Chem. Lett. 9 (2018) 4407–4412, https://doi.org/10.1021/acs.jpclett.8b01601.

[19] Y. Chen, K. Chen, J. Fu, A. Yamaguchi, H. Li, H. Pan, J. Hu, M. Miyauchi, M. Liu, Recent advances in the utilization of copper sulfide compounds for electrochemical CO2 reduction, Nano Mater. Sci. (2019), https://doi.org/10.1016/j.nanoms.2019.10.006.

[20] Z. Zhao, X. Peng, X. Liu, X. Sun, J. Shi, L. Han, G. Li, J. Luo, Efficient and stable electroreduction of CO2 to CH4 on CuS nanosheet arrays, J. Mater. Chem. A. 5 (2017) 20239–20243, https://doi.org/10.1039/C7TA05507B.

[21] T.T. Zhuang, Z.Q. Liang, A. Seifitokaldani, Y. Li, P. De Luna, T. Burdyny, F. Che, F. Meng, Y. Min, R. Quintero-Bermudez, C.T. Dinh, Y. Pang, M. Zhong, B. Zhang, J. Li, P.N. Chen, X.L. Zheng, H. Liang, W.N. Ge, B.J. Ye, D. Sinton, S.H. Yu, E. H. Sargent, Steering post-C-C coupling selectivity enables high efficiency electroreduction of carbon dioxide to multi-carbon alcohols, Nat. Catal. 1 (2018) 421–428, https://doi.org/10.1038/s41929-018-0084-7.

[22] P. Shao, S. Ci, L. Yi, P. Cai, P. Huang, C. Cao, Z. Wen, Hollow CuS microcube electrocatalysts for CO2 reduction reaction, ChemElectroChem 4 (2017) 2593–2598, https://doi.org/10.1002/celc.201700517.

[23] W. Van Der Stam, A.C. Berends, C. De Mello Donega, Prospects of colloidal copper chalcogenide nanocrystals, ChemPhysChem 17 (2016) 559–581, https://doi.org/10.1002/cphc.201500976.

[24] P. Munnik, P.E. De Jongh, K.P. De Jong, Recent developments in the synthesis of supported catalysts, Chem. Rev. 115 (2015) 6687–6718, https://doi.org/10.1021/cr500486u.
[25] R. Van Den Berg, G. Prieto, G. Korpershoek, L.I. Van Der Wal, A.J. Van Bunningen, S. Lægsgaard-Jørgensen, P.E. De Jongh, K.P. De Jong, Structure sensitivity of Cu and CuZn catalysts relevant to industrial methanol synthesis, Nat. Commun. 7 (2016), https://doi.org/10.1038/ncomms13057.
[26] P. Munnik, M. Wolters, A. Gabrielsson, S.D. Pollington, G. Headdock, J.H. Bitter, P. E. De Jongh, K.P. De Jong, Copper nitrate redispersion to arrive at highly active silica-supported copper catalysts, J. Phys. Chem. C 115 (2011) 14698–14706, https://doi.org/10.1021/jp111778g.
[27] G. Wang, R. van den Berg, C. de Mello Donega, K.P. de Jong, P.E. de Jongh, Silica-supported Cu2O nanoparticles with tunable size for sustainable hydrogen generation, Appl. Catal. B Environ. 192 (2016) 199–207, https://doi.org/10.1016/J.APCATB.2016.03.044.
[28] A.L. Patterson, The scherrer formula for X-ray particle size determination, Phys. Rev. 56 (1939) 978–982, https://doi.org/10.1103/PhysRev.56.978.
[29] J. Li, F. Che, Y. Pang, C. Zou, J.Y. Howe, T. Burdyny, J.P. Edwards, Y. Wang, F. Li, Z. Wang, P. De Luna, C.T. Dinh, T.T. Zhuang, M.I. Saidaminov, S. Cheng, T. Wu, Y. Z. Finfrock, L. Ma, S.H. Hsieh, Y.S. Liu, G.A. Botton, W.F. Pong, X. Du, J. Guo, T. K. Sham, E.H. Sargent, D. Sinton, Copper adparticle enabled selective electrosynthesis of n-propanol, Nat. Commun. 9 (2018), https://doi.org/10.1038/s41467-018-07032-0.
[30] ICDD (2019) PDF-4+ 2019 (Database), Edited by Dr. Soorya Kabekkodu, Int. Cent. Diffr. Data, Newt. Square, PA, USA. (n.d.).
[31] J. Grau, M. Akinc, Synthesis of nickel sulfide powders by thioacetamide in the presence of urea, J. Am. Ceram. Soc. 80 (2005) 941–951, https://doi.org/10.1111/j.1151-2916.1997.tb02925.x.
[32] J. Grau, M. Akinc, Synthesis of nickel sulfide by homogeneous precipitation from acidic solutions of thioacetamide, J. Am. Ceram. Soc. 79 (1996) 1073–1082, https://doi.org/10.1111/j.1151-2916.1996.tb08550.x.
[33] L. Bai, X. Ye, C. Song, H. Chen, B. Cai, Y. Bai, C. Xu, Z. Li, The surfactant-free synthesis of hollow CuS nanospheres: via clean Cu2O templates and their catalytic oxidation of dye molecules with H2O2, RSC Adv. 6 (2016) 83885–83889, https://doi.org/10.1039/c6ra19447h.
[34] W. Tang, A.A. Peterson, A.S. Varela, Z.P. Jovanov, L. Bech, W.J. Durand, S. Dahl, J. K. Nørskov, I. Chorkendorff, The importance of surface morphology in controlling the selectivity of polycrystalline copper for CO2 electroreduction, Phys. Chem. Chem. Phys. 14 (2012) 76–81, https://doi.org/10.1039/c1cp22700a.
[35] N.J. Firet, M.A. Blommaert, T. Burdyny, A. Venugopal, D. Bohra, A. Longo, W. A. Smith, Operando EXAFS study reveals presence of oxygen in oxide-derived silver catalysts for electrochemical CO 2 reduction, J. Mater. Chem. A. 7 (2019) 2597–2607, https://doi.org/10.1039/c8ta10412c.
[36] A.D. Handoko, F. Wei, Jenndy, B.S. Yeo, Z.W. Seh, Understanding heterogeneous electrocatalytic carbon dioxide reduction through operando techniques, Nat. Catal. 1 (2018) 922–934, https://doi.org/10.1038/s41929-018-0182-6.
[37] A. Eilert, F.S. Roberts, D. Friebel, A. Nilsson, Formation of copper catalysts for CO2 reduction with high Ethylene/Methane product ratio investigated with in situ X-ray absorption spectroscopy, J. Phys. Chem. Lett. 7 (2016) 1466–1470, https://doi.org/10.1021/acs.jpclett.6b00367.
[38] J.S. Yoo, R. Christensen, T. Vegge, J.K. Nørskov, F. Studt, Theoretical insight into the trends that guide the electrochemical reduction of carbon dioxide to formic acid, ChemSusChem 9 (2016) 358–363, https://doi.org/10.1002/cssc.201501197.
[39] T. Cheng, H. Xiao, W.A.G. Iii, Reaction mechanisms for the electrochemical reduction of CO 2 to CO and formate on the Cu(100) surface at 298 K from quantum mechanics free energy calculations with explicit water, J. Am. Chem. Soc. 138 (2016) 25, https://doi.org/10.1021/jacs.6b08534.
[40] A. Loiudice, P. Lobaccaro, E.A. Kamali, T. Thao, B.H. Huang, J.W. Ager, R. Buonsanti, Tailoring copper nanocrystals towards C2 products in electrochemical CO2 reduction, Angew. Chemie - Int. Ed. 55 (2016) 5789–5792, https://doi.org/10.1002/anie.201601582.
[41] R. Reske, H. Mistry, F. Behafarid, B. Roldan Cuenya, P. Strasser, Particle size effects in the catalytic electroreduction of CO2 on Cu nanoparticles, J. Am. Chem. Soc. 136 (2014) 6978–6986, https://doi.org/10.1021/ja500328k.